

# MOANA: Multi-Radar Dataset for Maritime Odometry and Autonomous Navigation Application

Journal Title  
XX(X):i–ix  
©The Author(s) 2024  
Reprints and permission:  
[sagepub.co.uk/journalsPermissions.nav](http://sagepub.co.uk/journalsPermissions.nav)  
DOI: 10.1177/ToBeAssigned  
[www.sagepub.com/](http://www.sagepub.com/)



Hyesu Jang<sup>1</sup> <sup>†</sup>, Wooseong Yang<sup>2</sup> <sup>†</sup>, Hanguen Kim<sup>3</sup>, Dongje Lee<sup>3</sup>, Yongjin Kim<sup>3</sup>, Jinbum Park<sup>3</sup>, Minsoo Jeon<sup>3</sup>, Jaeseong Koh<sup>3</sup>, Yejin Kang<sup>3</sup>, Minwoo Jung<sup>2</sup>, Sangwoo Jung<sup>2</sup>, Chng Zhen Hao<sup>4</sup>, Wong Yu Hin<sup>4</sup>, Chew Yihang<sup>4</sup>, and Ayoung Kim<sup>2</sup>

## Abstract

Maritime environmental sensing requires overcoming challenges from complex conditions such as harsh weather, platform perturbations, large dynamic objects, and the requirement for long detection ranges. While cameras and LiDAR are commonly used in ground vehicle navigation, their applicability in maritime settings is limited by range constraints and hardware maintenance issues. Radar sensors, however, offer robust long-range detection capabilities and resilience to physical contamination from weather and saline conditions, making it a powerful sensor for maritime navigation. Among various radar types, X-band radar (e.g., marine radar) is widely employed for maritime vessel navigation, providing effective long-range detection essential for situational awareness and collision avoidance. Nevertheless, it exhibits limitations during berthing operations where close-range object detection is critical. To address this shortcoming, we incorporate W-band radar (e.g., Navtech imaging radar), which excels in detecting nearby objects with a higher update rate. We present a comprehensive maritime sensor dataset featuring multi-range detection capabilities. This dataset integrates short-range LiDAR data, medium-range W-band radar data, and long-range X-band radar data into a unified framework. Additionally, it includes object labels for oceanic object detection usage, derived from radar and stereo camera images. The dataset comprises seven sequences collected from diverse regions with varying levels of estimation difficulty, ranging from easy to challenging, and includes common locations suitable for global localization tasks. This dataset serves as a valuable resource for advancing research in place recognition, odometry estimation, simultaneous localization and mapping (SLAM), object detection, and dynamic object elimination within maritime environments. Dataset can be found in following link: <https://sites.google.com/view/rpmmoana>

## Keywords

Dataset, Maritime, Radar, LiDAR, Object Detection, Place Recognition, Odometry, SLAM

## 1 Introduction

As autonomous vehicles gain prominence within the field of robotics, the demand for research and development continues to rise. Many advancements in this domain have been driven by high-quality datasets featuring well-calibrated sensor configurations and carefully designed trajectories. From ground-driving datasets (Geiger et al. 2012) to aerial datasets, and from imaging sensors to range sensors (Kim et al. 2020), various datasets have been made publicly available to support robust advancements in autonomous systems.

However, exploring oceanic environments remains a significant challenge. While high-quality datasets are essential for impactful research, the availability of maritime datasets lags behind current demands due to the complexities associated with sensor configuration and the inherent challenges of data collection in maritime environments.

The existing maritime dataset (Chung et al. 2023) represents a significant contribution, providing navigational data from marine radar only with X-band wavelength, along with LiDAR, and camera systems and ground truth information. While this dataset marks a pioneering step

for maritime research, it lacks regional diversity, limiting its applicability across varied navigational environments. Understanding this limitation requires familiarity with the stages of vessel navigation: berthing at a port, sailing in open waters, and docking. While near-range detection is critical during berthing and docking, long-range detection is essential for open-water navigation. Existing datasets provide limited coverage of such wide-open maritime areas, restricting utility for radar navigation research.

Moreover, the existing dataset faces limitations in sensor capabilities, as the canal environment is insufficient to represent radar-based marine navigation. Traditional marine radars (X-band) are pivotal in ensuring situational awareness and preventing collisions in wide oceanic areas with their

<sup>1</sup> Institute of Advanced Machines and Design, SNU, Seoul, S. Korea

<sup>2</sup> Dept. of Mechanical Engineering, SNU, Seoul, S. Korea

<sup>3</sup> SeadroneX, Seoul, S. Korea

<sup>4</sup> Defence Science and Technology Agency, Singapore

<sup>†</sup>Two authors contributed equally.

## Corresponding author:

Ayoung Kim, Dept. of Mechanical Engineering, SNU, Seoul, S. Korea  
Email: ayoungk@snu.ac.kr

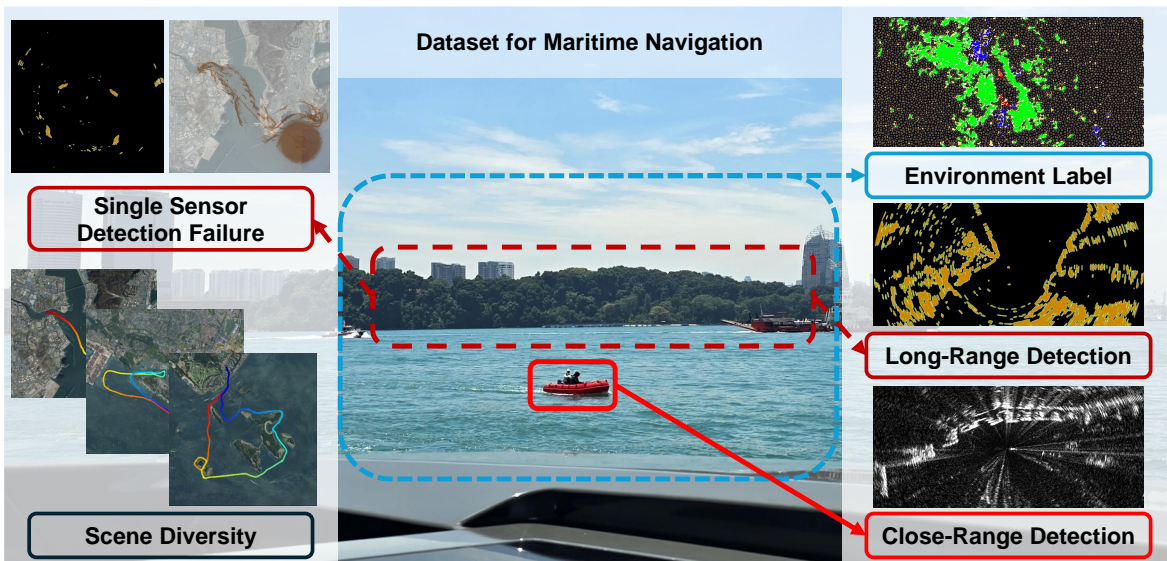


**Figure 1.** Overview of the MOANA dataset. To address the limitations of individual sensor performance in maritime environments, we enhanced the sensor system by integrating complementary sensors to improve both range and resolution. Data acquisition was carried out across diverse scenarios using multiple sensor types, providing a robust dataset with annotated labels for the development of learning-based algorithms.

long-range detection ability. Despite its broad sensing range, X-band radars are limited in detecting short-range objects and often suffer from multipath interference and noise in the canal area, as illustrated in Figure 1. Therefore, it is necessary to explore alternative sensors for short-range detection. While LiDAR has proven effective for this short-range detection, it is not a sustainable solution in maritime environments due to challenges like sea fog, corrosion, and the necessity for frequent cleaning during extended voyages. We have found that W-band radar can be a superior alternative to LiDAR for short-range and wide-area detection in marine environments. W-band radar, often called scanning radar, has previously demonstrated its potential exclusively in ground vehicle applications due to its extended detection range compared to LiDAR. Its higher resolution and environmentally robust detection ability can mitigate the shortcomings of existing sensors in the maritime domain. Nevertheless, there have been no reports of its use in marine environments.

Overcoming the aforementioned limitations in the existing marine dataset, we present a maritime navigational dataset with a novel sensor configuration tailored for various maritime environments. We integrated multiple radar systems into the dataset, combining W-band radar with X-band radar to ensure comprehensive coverage. This novel configuration enables us to address both long-range and short-range detection challenges, enhancing the data continuity for diverse maritime navigation scenarios. The expected influences of our dataset are written below:

1. The MOANA dataset represents the first multi-radar (X-band and W-band) dataset collected in a maritime environment. The X-band radar is utilized for wide-area detection, while the W-band radar delivers high-resolution imaging for near-port areas. Their differing bandwidths allow for seamless integration, and our benchmark results also demonstrate that a complementary sensor configuration enables robust navigation across various maritime conditions. Our

dataset also provides cameras and LiDAR data for the ground truth labels of detected objects, encouraging diverse fusion strategies for vessel navigation tasks: berthing, sailing, and docking.

2. The MOANA dataset tackles maritime navigation tasks in varying environments. Our dataset encompasses both structured port and unstructured ocean and island settings with varying vessel sizes. This large spectrum of scene diversity underscores the necessity of navigation algorithms operating in multifarious environments. Additionally, the loops and overlaps between sequences support inter and intra-place recognition in maritime environments.
3. The MOANA dataset provides a series of challenges designed to evaluate the robustness of existing navigation algorithms. The sequences include objectless data, ghost detections caused by multipath noise, and the presence of large dynamic objects. All are aimed at preventing unpredictable conditions that can affect the robustness of navigation systems.

## 2 Related works

This section summarizes the existing maritime dataset focused on cameras and LiDAR and examines W-band datasets that have so far been limited to ground-based usage in advance of introducing the first multi-radar dataset to incorporate the W-band radar from maritime environments. The brief summarization is depicted in Table 1.

### 2.1 Marine Robotics Datasets

The development of maritime environment datasets also began with vision-based approaches. Early efforts included a camera-infrared dataset for day and low-light conditions (Zhang et al. 2015) and a bird's-eye-view maritime surveillance camera dataset (Ribeiro et al. 2017). Additionally, maritime imagery for learning-based models has been provided (Bovcon et al. 2019). Attempts to integrate camera,

**Table 1.** Radar Dataset Comparison

| Name   | W-Band | Radar X-Band | 4D | Navigation Loop Closure | Scene Diversity | Object Detection Label | Ground Truth | Route Complexity | Environment |
|--|--------|--------------|----|-------------------------|-----------------|------------------------|--------------|------------------|-------------|
| Oxford Radar<br><a href="#">Barnes et al. (2020)</a> | ✓      | ✗            | ✗  | ✓                       | Identical       | ✗                      | ✗            | ***              | Land        |
| MulRan<br><a href="#">Kim et al. (2020)</a>          | ✓      | ✗            | ✗  | ✓                       | **              | ✗                      | ✗            | ***              | Land        |
| Radiate<br><a href="#">Sheeny et al. (2021)</a>      | ✓      | ✗            | ✗  | ✓                       | **              | ✓                      | ✓            | **               | Land        |
| Boreas<br><a href="#">Burnett et al. (2023)</a>      | ✓      | ✗            | ✗  | ✓                       | *               | ✓                      | ✓            | **               | Land        |
| OODR<br><a href="#">Gadd et al. (2024)</a>           | ✓      | ✗            | ✗  | ✓                       | ***             | ✗                      | ✗            | **               | Land        |
| USVInland<br><a href="#">Cheng et al. (2021)</a>     | ✗      | ✗            | ✓  | ✓                       | ***             | ✓(Water)               | ✓            | **               | Waterway    |
| Pohang Canal<br><a href="#">Chung et al. (2023)</a>  | ✗      | ✓            | ✗  | ✗                       | Identical       | ✗                      | ✗            | *                | Maritime    |
| <b>MOANA</b>   | ✓      | ✓            | ✗  | ✓                       | ***             | ✓                      | ✓            | ***              | Maritime    |

LiDAR, and single-chip radar on unmanned surface vehicles were made (Cheng et al. 2021), but the single-chip radar system has insufficient resolution for oceanic environments. Recently, (Chung et al. 2023) introduced a multi-purpose marine radar dataset. While camera and LiDAR data exhibit limitations in open water scenarios due to detection range constraints, including X-band marine radar in this dataset addresses these shortcomings, offering a more comprehensive solution for maritime applications. Unlike existing maritime datasets, the MOANA dataset incorporates both X-band and W-band radar to enhance the robustness of detectability for diverse maritime navigation tasks.

## 2.2 W-band Radar Datasets

The use of W-band radar has been confined to ground vehicle datasets. Pioneering radar datasets, including MulRan (Kim et al. 2020) and the Oxford Radar Robotcar (Barnes et al. 2020), have established radar as a viable sensor for navigation. Following these foundational efforts, datasets have been extended to include various challenging environments, such as adverse weather conditions (Sheeny et al. 2021), multi-season driving (Burnett et al. 2023), and complex terrains (Gadd et al. 2024). The MOANA dataset is differentiated from the existing W-band radar datasets, exploiting W-band radar in the maritime domain for the first time. Consequently, the MOANA dataset serves as a milestone to verify the potential of the W-band radar in vessel navigation research.

## 3 System Overview

### 3.1 System Configuration

Due to the variability in conditions across different oceanic environments, identical sensor configurations could not be applied across all locations. As a result, our dataset was collected using two distinct vessels. The detailed sensor configuration is provided in Figure 2. The first sequence, Port, was captured using a small fishing boat, while the Island sequence was recorded aboard a larger yacht. The primary sensors in the dataset are two radars: X-band and W-band. Global positioning of the system was provided by a GNSS receiver using Dual GPS mode. Additionally, two

**Table 2.** The radar specifications utilized in dataset

| Dataset     | Manufacture | Model      | Range Resolution | Range |
|-------------|-------------|------------|------------------|-------|
| Port,Island | SIMRAD      | HALO4      | 3m               | 1852m |
| Port        | Navtech     | RAS6-DEV-A | 0.175m           | 600m  |
| Island      | Navtech     | RAS6-DEV-X | 0.175m           | 600m  |

cameras and a LiDAR were integrated to support multimodal navigational tasks.

### 3.2 Sensor Calibration

The base for the yacht is established using the GNSS data. all the extrinsic calibration data are included in the calibration.

**3.2.1 Multiple Radar Calibration** Two radar data are provided as image types that are discriminated against with image pixels. We convert the W-band polar coordinate images to Cartesian coordinates with the same resolution as the X-band radar and perform the extrinsic calibration by considering the overlap of the prominent features at the pixel level. Since the two radars are structurally incapable of providing information in the vertical direction, vertical extrinsic calibration was conducted using a CAD model.

**3.2.2 LiDAR W-band Radar Camera Calibration** For the LiDAR and W-band radar calibration, we utilized the phase correlation between LiDAR and W-band radar, similar to MulRan (Kim et al. (2020)). We first make the polar image from the bird-eye-view scan of LiDAR. Due to the limited detection range of LiDAR, we leveraged the LiDAR scan near the port area. Then, we exploited the phase correlation approach between the polar images of LiDAR and W-band radar to compute the extrinsic parameters of x, y, and yaw components. The other extrinsic parameter components were achieved with our sensor setup’s CAD model.

The intrinsic calibration of the camera was performed using a known pattern target board to estimate the distortion coefficients and intrinsic parameters. The extrinsic calibration between the camera and LiDAR was conducted through the matching of stationary planar objects with known geometries. The initial transformation for the extrinsic calibration was given by the CAD model.

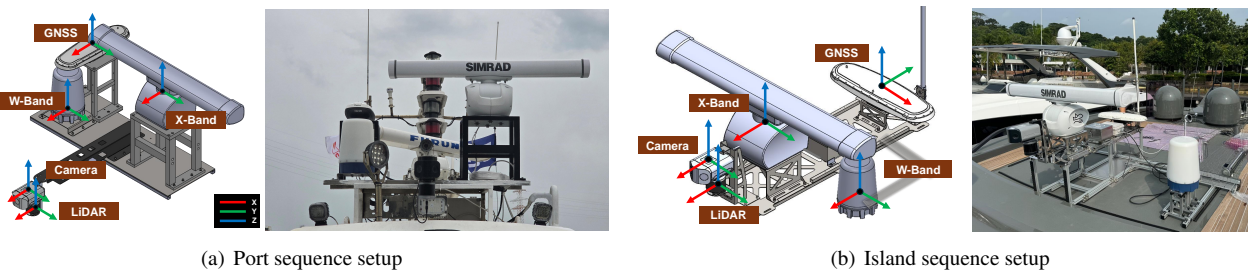


**Figure 2.** Modeling and real-world capture setups for two distinct configurations. The primary difference between the hardware setups is the orientation of the GNSS receiver: in the port sequence, the vessel's forward direction aligns with the x-axis, whereas the island sequence is rotated by 90°. Additionally, the W-band radar is positioned on the right side in the port sequence and on the left side in the island sequence. Detailed configurations are provided in the calibration files.

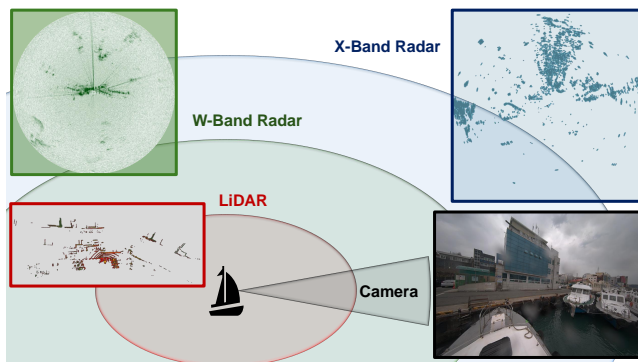


**Figure 3.** Composition of sensor types and example images. Radar sensors generate 360-degree scanning bird's-eye view images, while LiDAR provides 360-degree point cloud data. The camera system captures stereo images in the forward direction.

## 4 MOANA Dataset

### 4.1 Data Composition

As detailed in Chap. 3.1, our dataset includes data from two different band radars, LiDAR, stereo camera, and GNSS Reciever. Figure. 3 provides the data sample with detection range comparison for each sensor. Both scanning radars and stereo cameras generate image data, making this dataset composed of four images for every data publication. To address potential challenges in managing large data volumes, we offer an individual file structure in *Sequence/sensor\_data/sensor\_type* directory, enabling users to download only the data relevant to their needs. Additionally, we provide a ROS-based data publisher to facilitate seamless access and integration of the dataset. An overview of the file structure is illustrated in Figure. 4.

**4.1.1 X-Band Radar** X-band radar data, commonly referred to as marine radar data, is stored as Cartesian coordinate image files. The radar's maximum range is set to 1 nautical mile for the Island sequences and 1 km for the Port sequences. To optimize sensor fusion efficiency, we fixed the sensor update rate at 1 Hz. Originally, the radar requires three seconds to complete a full 360-degree rotation. However, the data provided updates one-third of the full image per second. This modification was implemented to reduce dynamic changes that occur over short time intervals, thereby enhancing the temporal resolution of the sensor data.

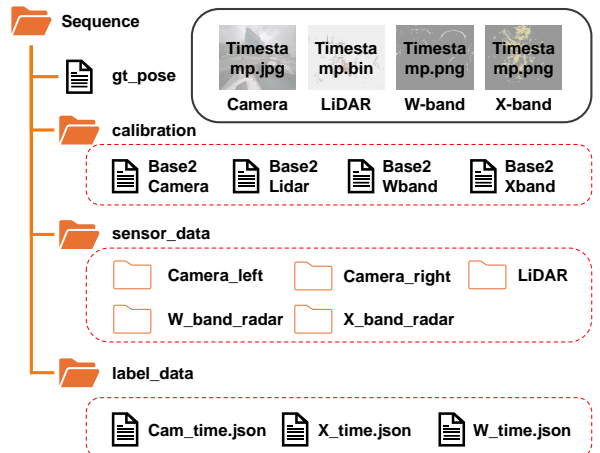


**Figure 4.** Data organization and file structure for each sequence of MOANA dataset. Ground truth poses are provided as text files. Extrinsic calibration parameters for the camera, LiDAR, and radars are defined relative to the base frame. Sensor data is available with distinguished file formats, such as PNG images. Additionally, labels for each frame are supplied as JSON files, each named according to the corresponding frame timestamp. For the stereo camera annotation, we denote the left camera as Cam0, and the right camera as Cam1 for JSON files.

**4.1.2 W-Band Radar** W-band radar, commonly referred to as imaging radar, was employed in our study using the Navtech RAS6 models. This radar system has a range of approximately 600 meters and provides data in the form of polar coordinate images. Two variants of the W-band radar were utilized for different experimental sequences. For the Port sequences, we used the RAS6-DEV-A model, characterized by radar rays that propagate horizontally, detecting objects at the same elevation level as the radar itself. In contrast, the Island sequences utilized the RAS6-DEV-X model, which emits rays capable of detecting objects below the radar's elevation. This adaptation was necessary to accommodate the vessel's size differences; specifically, the vessel in the Island sequences has a height of approximately 6 meters, double that of the vessel used in the Port sequences. Although W-band radar is traditionally utilized for ground vehicle navigation, it proves to be highly advantageous for maritime applications. It offers superior resolution in detecting surrounding environments compared to X-band radar and exhibits greater robustness than sensors

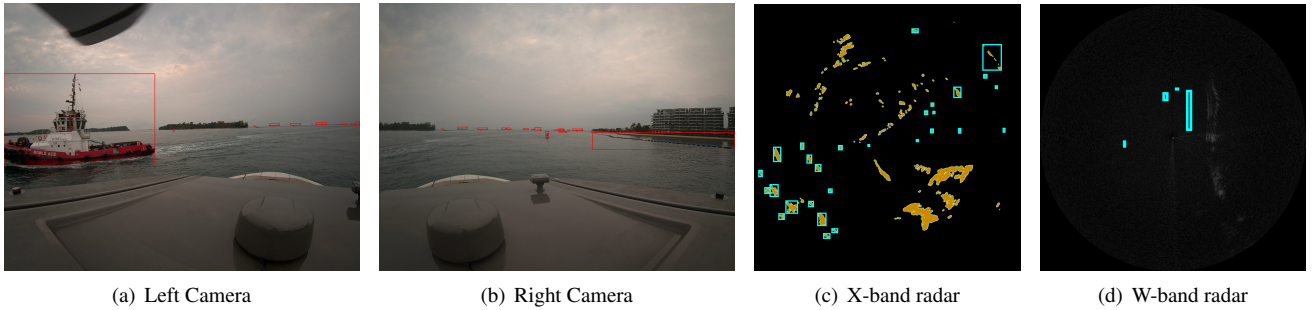


**Figure 5.** Examples of 2D annotation for the stereo camera, X-band radar, and W-band radar data. (a,b) The bounding boxes of the detected objects (vessels, buoys) are represented as red boxes. (c,d) yellow and gray pixels are from the X-band and W-band radar each, and the bounding boxes of detected objects are highlighted with "cyan" color.

based on optical wavelengths. The specification of the radar configuration is detailed in Table 2.

**4.1.3 LiDAR and Camera** To validate the environmental conditions during sensor data acquisition, we additionally equipped the vessel with fundamental navigational sensors, LiDAR and a stereo camera. Due to LiDAR’s limited detection range, most of its data is sparse except in the berthing regions. The primary reason for incorporating LiDAR into this dataset is to assess precision during berthing maneuvers, where radar saturation can occur.

The stereo camera data allowed us to detect nearby vessels and structures even when operating in open ocean. This visual data serves as ground truth for object labeling tasks. Estimating visual odometry using only the stereo camera is challenging in oceanic environments due to the scarcity of discernible objects; however, this presents an additional challenge for researchers to address.

**4.1.4 Calibration and Ground Truth** The extrinsic calibration files and ground truth positions from the GNSS receiver are provided as text files. We employed the Hemisphere V500 GNSS receiver, which delivers precise positioning along with heading information. While the receiver’s native update frequency is 10 Hz, we have synchronized the data with other sensors to a 1 Hz update rate in our dataset. The GNSS receiver serves as the reference frame for the vessel model, and the extrinsic parameters are calculated based on the correlation with this base frame.

**4.1.5 Annotation Label** We provide the ground truth of 2D bounding box annotations for detected objects in X-band radar, W-band radar, and stereo images in the Single Island sequence. The annotations in the JSON file contain  $[timestamp, id, category\_id, xmin, ymin, width, height]$ .  $id$  represents the tracked object ID that is detected in consecutive frames. The  $category\_id$  is fixed at a value of 1, corresponding to the objects that should be avoided during navigation (e.g. vessels or buoys). The  $[xmin, ymin, width, height]$  parameters represent the bounding box location and dimensions of the detected objects in each image. For the W-band radar, the locations of the bounding box are represented in  $1024 \times 1024$  Cartesian image coordinates, which are converted from the polar coordinate image. Figure 5 depicts an example of provided 2D annotations in each images.

## 4.2 Sequences

MOANA dataset encompasses two distinct regional environments: South Korea and Singapore. The data collected in South Korea is from Ulsan, an area characterized by predominantly industrial structures. The port area is developed for cargo transport, and the surroundings are densely packed with factory sites and artificial structures. This provided a highly structured environment, which we refer to as the Port sequence.

In contrast, the dataset from Singapore is collected in the Harborfront area, representing a largely unstructured environment. Apart from the berthing point, the surroundings are dominated by natural elements such as trees and rocks, making localization algorithms more challenging. Given the varying sizes of islands in this region, we have designated this sequence as the Island sequence. A detailed explanation of each sequence and the associated challenges is provided below.

**4.2.1 Port Sequence:** The Port sequences represent a highly structured, industrial environment characterized by strong and consistent detections of the surrounding area. This sequence is primarily designed for odometry or SLAM applications, where generating a reliable map of the port is the main objective. It is the most straightforward sequence for algorithm testing, with the primary challenge being the mitigation of wave-induced wobble, which leads to inconsistencies in radar data. As radar systems rely on reflected signals, this wobble can disrupt the Radar Cross Section (RCS) continuity of sensor measurements.

Additionally, the presence of numerous anchored large vessels introduces both opportunities and challenges for tracking. The radar-reflective coatings on these ships make them ideal objects for tracking in open water. However, proximity to these vessels can lead to significant multipath effects, complicating the tracking process.

**(i) Near Port:** In the Near Port sequence, the dataset primarily emphasizes W-band radar due to its superior performance in short-range detection, as X-band radar exhibits limitations in this condition. W-band radar is, therefore, the predominant sensor for capturing the surrounding environment in these sequences. A significant challenge arises at the halfway point, where severe multipath effects generate ghost objects, a critical obstacle to achieving robust navigation.

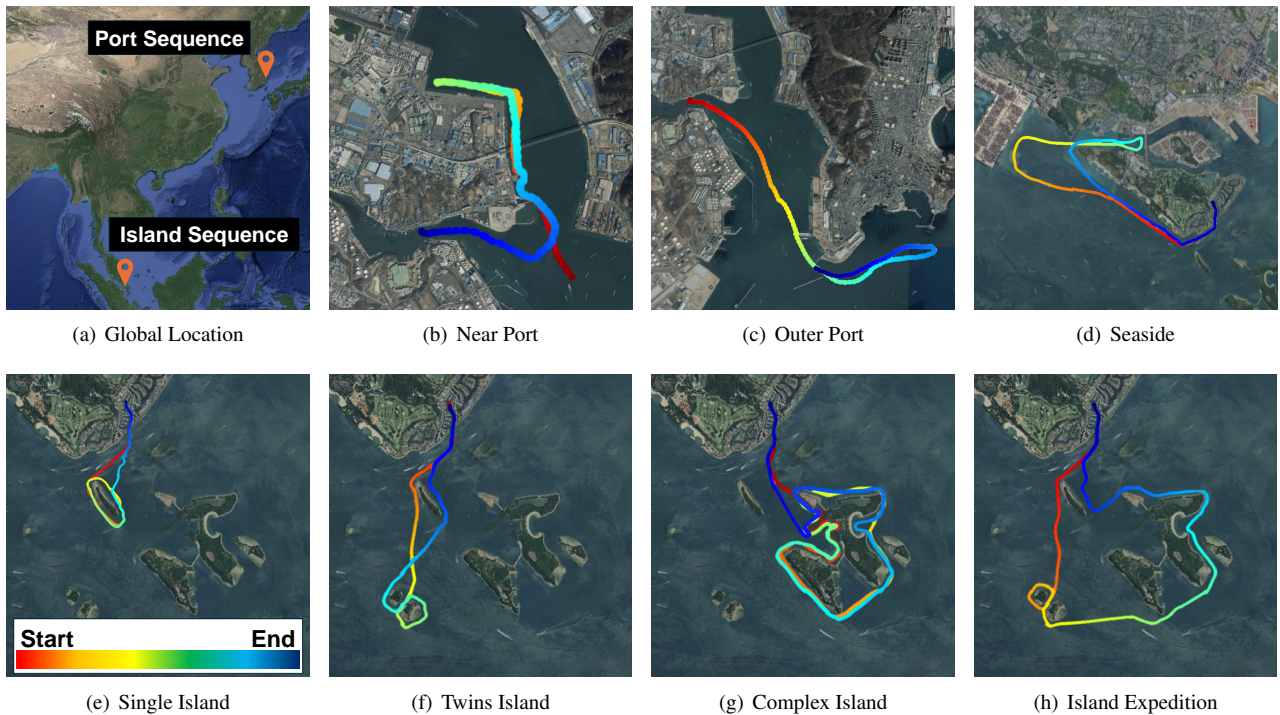


**Figure 6.** Ground truth trajectories for all sequences. The **Port** sequences (b, c) were collected in South Korea, while the **Seaside** and **Island** sequences (d, e, f, g, h) were acquired in Singapore. All sequences share instant common locations except for the **Island Expedition** sequence (h), which encompasses three sub-sequences (e, f, g). Trajectories commence in red and terminate in blue.

**(ii) Outer Port:** In contrast, the Outer Port sequence focuses on X-band radar, as W-band radar's limited detection range renders it ineffective in certain areas. For both odometry and mapping tasks, X-band radar serves as the primary sensor. However, in the narrow-loop regions, W-band radar can be effectively utilized, provided its characteristics are leveraged appropriately.

**4.2.2 Island Sequence:** The Island sequences present an unstructured, sporadic environment dominated by natural elements. Due to these features, surrounding detections are inconsistent, making it challenging to recognize the same locations reliably. The dataset includes three distinct island environments: single island, twins island, and complex island. Each sequence contains overlapping areas with others, facilitating global place recognition across the dataset. In addition to island sequences, the sequence also includes seaside areas, providing a mix of both unstructured natural environments and more structured coastal regions.

**(i) Single Island:** The Single Island sequence features the shortest route in the island dataset, consisting of a simple loop around the island. The yacht completes two laps before returning to the berthing point.

**(ii) Twins Island:** Twins island is located at the farthest distance and experiences sporadic data loss in the W-band radar. However, as the vessel navigates through the narrow waterway between the islands, W-band radar becomes essential for robust positioning and detection, compensating for the limitation of the X-band radar.

**(iii) Complex Island:** Complex island is the largest island, which is suited for evaluating odometry algorithms. Long, circular route makes the distance between

the starting and end points a valuable metric for assessing marine odometry performance.

**(iii) Island Expedition:** Island Expedition encompasses all three islands but only includes partial segments from each. This dataset is ideal for testing global localization algorithms.

**(iv) Seaside:** Lastly, the Seaside sequence incorporates both beachside environments and a container loading zone. This sequence is particularly useful for analyzing the impact of both structured and unstructured environments within a single dataset.

## 5 Radar Odometry Benchmark

### 5.1 W-band radar odometry (CFEAR)

For the benchmark test of W-band radar odometry, we employed the CFEAR (Adolfsson et al. 2022) method, a state-of-the-art approach for W-band radar odometry estimation. Although our goal was to evaluate the entire trajectory, empty-object data in certain areas made this infeasible. As a result, the W-band radar odometry had to be limited to sections where the vessel remained near the shoreline. The results are depicted in Figure 7 and Table 3.

In the Port sequence, we achieved reasonable odometry estimation from Near Port data. However, as intended, the majority of W-band radar images in the Outer Port data were blank, precluding meaningful results from this sequence. This design choice highlights the necessity of incorporating additional sensors to overcome inherent limitations and ensure stable vessel navigation. For the Island sequence, there were sporadic challenges that make it difficult to conduct odometry estimation. We provide

**Table 3.** Absolute Trajectory Error for W-band and X-band radars. Due to challenging data in other sequences, only the Near Port sequence was evaluated using both W-band and X-band radar odometry algorithms. The W-band radar demonstrates lower error in the Near Port sequence, attributable to its superior close-range detection accuracy compared to the X-band radar. In contrast, the X-band radar exhibits robust performance across all other sequences not covered by the W-band radar sensor.

| Method                                  | Radar  | Port Sequence |            | Island Sequence |              |                |                   |         |
|---|--------|---------------|------------|-----------------|--------------|----------------|-------------------|---------|
|   |        | Near Port     | Outer Port | Single Island   | Twins Island | Complex Island | Island Expedition | Seaside |
| <b>CFEAR</b><br>Adolfsson et al. (2022) | W-Band | 20.35         | -          | -               | -            | -              | -                 | -       |
| <b>LodeStar</b><br>Jang et al. (2024)   | X-Band | 63.48         | 78.92      | 41.59           | 53.17        | 22.88          | 130.48            | 35.81   |

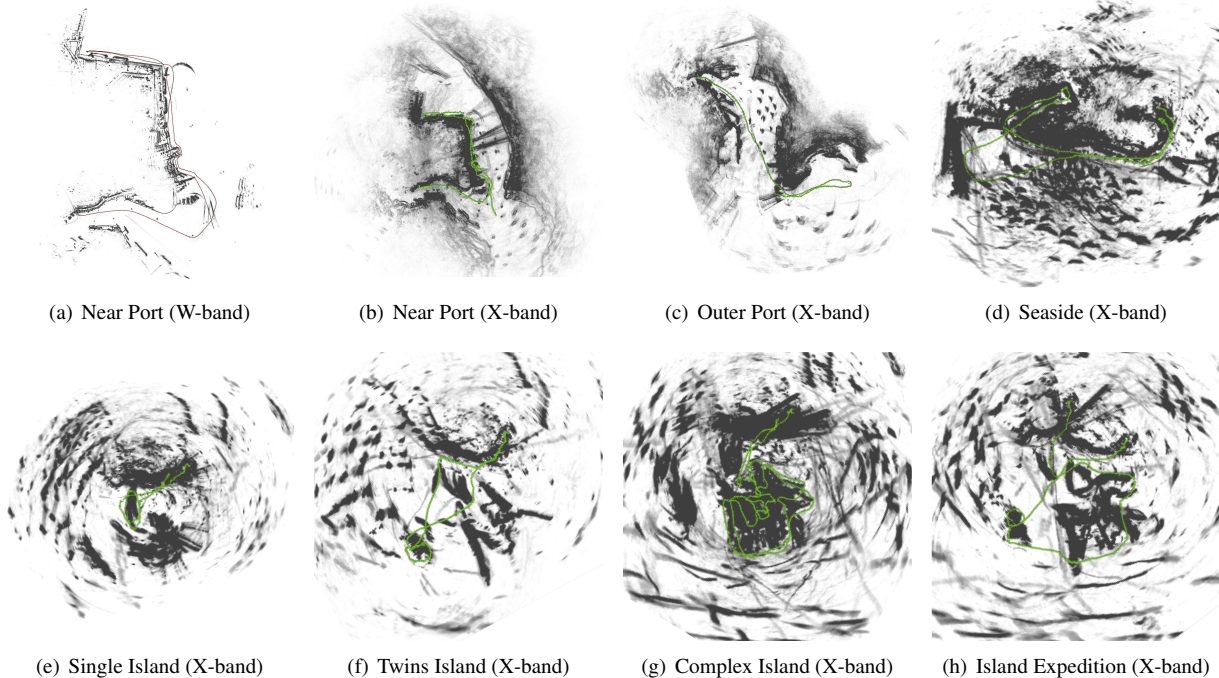


**Figure 7.** W-band and X-band radar odometry/mapping results. The Port sequences achieve promising odometry performance due to the presence of continuous features such as walls and bridges. In contrast, the Island sequences, which lack these features, show insufficient performance in W-band radar odometry. However, X-band radar still demonstrates superior performance compared to W-band radar odometry. In near-land areas, adjusting the vessel's pose using W-band radar could further enhance odometry accuracy.

test figure in Figure 8 to depict our traversal around the Single Island with W-band radar odometry estimation. While berthing area features were successfully captured, ambiguous detection of unstructured environments such as trees and sand hindered frame-to-frame matching, presenting challenges that warrant further investigation. In summary, we observed that the W-band radar can accurately depict surrounding environments, but its short-range limitation impedes the observation of movement between islands. This result underscores the need for sensor fusion with longer-range sensors, which are included in this dataset. Integrating data from the X-band radar could facilitate continuous vessel motion tracking.

## 5.2 X-band radar odometry (*LodeStar*)

For X-band radar odometry estimation, we employed the LodeStar (Jang et al. 2024) algorithm, which is a state-of-the-art method in this domain. Unlike the W-band radar benchmark test, we utilized the full dataset for the X-band radar benchmark since the surrounding data were comprehensively captured. The only significant challenges

arose from data saturation when the vessel approached too closely to territorial regions, causing multipath noise and false alarms in the sensor images.

In the Port sequence data, we observed robust odometry estimation despite some radar saturation occurring in the Near Port sequence. However, the saturation issues in the Island sequence were not managed, leading to tracking loss during odometry estimation. To achieve more accurate and robust odometry, incorporating near-range data from other sensors such as W-band radar can provide enhanced results.

## 6 Radar Object Detection in Maritime Environments

Unfortunately, there is a lack of publicly available object detection methods for both X-band and W-band radar in the maritime environment. Typically, existing object detection algorithms in the W-band radar are primarily designed for ground vehicles or pedestrian detection in land environments, which are not adaptable for marine vessel detection tasks. As the MOANA dataset demonstrates

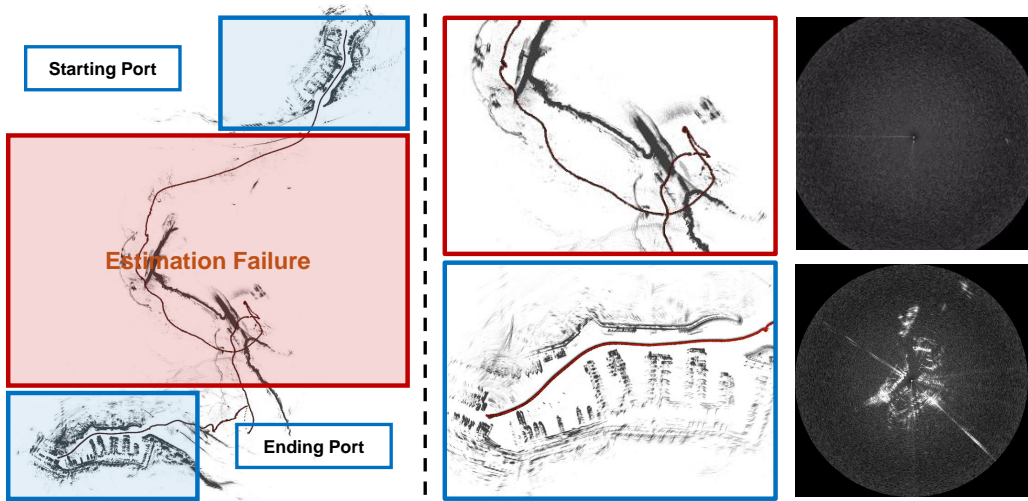


**Figure 8.** Odometry estimation results using W-band radar for the Single Island sequence. The W-band radar successfully generates reliable odometry and mapping outcomes with existing methods near the berthing area (blue) of the Single Island sequence. However, tracking loss frequently occurs when processing unstructured and featureless data (red).

the potential application of W-band radar for short-range detection in maritime navigation tasks, we expect that our dataset will contribute to developing oceanic radar object detection algorithms.

## 7 Conclusion

MOANA presents the first maritime multi-radar dataset incorporating scanning radars of different bandwidths. Our dataset facilitates the use of W-band radar in oceanic environments while maintaining vessel ego-motion tracking by leveraging existing X-band radar. Addressing the limitations of W-band radar, W-band radar also mitigates the vulnerability of X-band radar during berthing operations. Our benchmark result also demonstrated that integrating the X-band and W-band radar can further enhance the performance of maritime navigation tasks such as berthing, sailing, and docking. Seven sequences in this dataset are expected to support advancements in autonomous navigation systems. In future updates, we aim to extend the dataset with sequences incorporating temporal variance to evaluate robustness under time-differentiated conditions.

## Acknowledgements

This work was supported by the Technology Innovation Program (1415187329, Development of autonomous driving connectivity technology based on sensor-infrastructure cooperation) funded By the Ministry of Trade, Industry & Energy (MOTIE, Korea), and the research in the Singapore region was supported by Defence Science and Technology Agency (DSTA)

## References

- Adolfsson D, Magnusson M, Alhashimi A, Lilienthal AJ and Andreasson H (2022) Lidar-level localization with radar? the cfear approach to accurate, fast, and robust large-scale radar odometry in diverse environments. *IEEE Transactions on robotics* 39(2): 1476–1495.
- Barnes D, Gadd M, Murcatt P, Newman P and Posner I (2020) The oxford radar robotcar dataset: A radar extension to the oxford robotcar dataset. In: *Proc. IEEE Intl. Conf. on Robot. and Automat.* pp. 6433–6438.
- Bovcon B, Muhovič J, Perš J and Kristan M (2019) The mastr1325 dataset for training deep usv obstacle detection models. In: *Proc. IEEE/RSJ Intl. Conf. on Intell. Robots and Sys.* pp. 3431–3438.
- Burnett K, Yoon DJ, Wu Y, Li AZ, Zhang H, Lu S, Qian J, Tseng WK, Lambert A, Leung KY, Schoellig AP and Barfoot TD (2023) Boreas: A multi-season autonomous driving dataset. *Intl. J. of Robot. Research* 42(1-2): 33–42.
- Cheng Y, Jiang M, Zhu J and Liu Y (2021) Are we ready for unmanned surface vehicles in inland waterways? the usvinland multisensor dataset and benchmark. *IEEE Robot. and Automat. Lett.* 6(2): 3964–3970.
- Chung D, Kim J, Lee C and Kim J (2023) Pohang canal dataset: A multimodal maritime dataset for autonomous navigation in restricted waters. *Intl. J. of Robot. Research* 42(12): 1104–1114.
- Gadd M, De Martini D, Bartlett O, Murcatt P, Towlson M, Widojo M, Muşat V, Robinson L, Panagiotaki E, Pramatarov G et al. (2024) Oord: The oxford offroad radar dataset. *arXiv preprint arXiv:2403.02845*.
- Geiger A, Lenz P and Urtasun R (2012) Are we ready for autonomous driving? the kitti vision benchmark suite. In: *Proc. IEEE Conf. on Comput. Vision and Pattern Recog.*
- Jang H, Jung M, Jeon MH and Kim A (2024) Lodestar: Maritime radar descriptor for semi-direct radar odometry. *IEEE Robotics and Automation Letters*.
- Kim G, Park YS, Cho Y, Jeong J and Kim A (2020) Mulran: Multimodal range dataset for urban place recognition. In: *Proc. IEEE Intl. Conf. on Robot. and Automat.* pp. 6246–6253.
- Ribeiro R, Cruz G, Matos J and Bernardino A (2017) A data set for airborne maritime surveillance environments. *IEEE Transactions on Circuits and Systems for Video Technology* 29(9): 2720–2732.
- Sheeny M, De Pellegrin E, Mukherjee S, Ahrabian A, Wang S and Wallace A (2021) Radiate: A radar dataset for automotive perception in bad weather. In: *2021 IEEE International*

- Conference on Robotics and Automation (ICRA). IEEE, pp. 1–7.
- Zhang MM, Choi J, Daniilidis K, Wolf MT and Kanan C (2015) Vais: A dataset for recognizing maritime imagery in the visible and infrared spectrums. In: *Proceedings of the IEEE conference on computer vision and pattern recognition workshops*. pp. 10–16.